

Numerical Investigation of Thermoelastic Crack Interactions in Various Materials using a Novel Enrichment Approach

Ayush Awasthi

Department of Mechanical Engineering,
National Institute of Technology, Hamirpur, 177005, Himachal Pradesh, India.
E-mail: ayush@nith.ac.in

Mohit Pant

Department of Mechanical Engineering,
National Institute of Technology, Hamirpur, 177005, Himachal Pradesh, India.
Corresponding author: mohitpant.iitr@gmail.com

(Received on May 31, 2023; Accepted on September 6, 2023)

Abstract

Crack interaction studies play a crucial role in understanding and predicting the fracture behaviour of various engineering components subjected to thermomechanical loads. The present work investigates the interaction effect of multiple cracks in different types of material subjected to thermoelastic loadings using Element free Galerkin method (EFGM). These materials include isotropic material, orthotropic material, functionally graded material, and layered material. These all materials are subjected to thermoelastic loads in presence of multiple cracks to investigate the effect of crack interactions. A novel modified Intrinsic enrichment has been proposed to precisely capture the interaction effect and stress fields in the presence of multiple cracks. The proposed algorithm has been tested for a benchmark problem and it produced better stress fields in comparison to the conventional EFGM procedure. Stress intensity factors corresponding to variations in crack parameters have been evaluated concerning with the primary crack. Results reveal that presence of multiple cracks alters the crack tip stress fields owing to the interaction effect i.e. shielding or amplification. Additionally, parameters such as crack length, crack orientation, distance between cracks, and domain properties greatly influence the stress intensity factor of the primary crack. These parameters exhibit varying behaviour under distinct circumstances, and their effects have been thoroughly analysed. Current work provides valuable insights into the effects of crack interactions in different media under thermoelastic loadings, thereby ensuring the structural integrity and durability of these materials for practical applications.

Keywords- Meshfree methods, Fracture, EFGM, Crack, Crack interaction, Thermoelastic, Stress intensity factor.

1. Introduction

Understanding the behaviour and integrity of materials under various conditions is a critical aspect of engineering. Complexity of applications in the modern world has led to the development of various types of materials like composites, graded materials etc. (Miteva, 2014; Awasthi et al., 2021). Most engineering components experience failures in both mechanical and thermal conditions during their operational lifespan. These combined thermo-mechanical loads generate singular stress fields around the regions of discontinuities like voids, cracks etc. Manufacturing and machining of such materials create some kinds of microcracks on the surface of materials thereby affecting their performance (Nusier & Newaz, 1998; Kolednik et al., 2010) These cracks act as regions of high-stress singularities which may lead to failure of components. Presence of one or multiple cracks in a component makes it vulnerable to high stresses. Proper estimation of stresses around these cracks is necessary for avoiding any catastrophic failure. Crack interaction studies play an important role in understanding the behaviour and integrity of materials under varying conditions (Ouinan et al., 2010; Yan & Miao, 2012). The interaction between multiple cracks within a structure can significantly affect its mechanical properties, like strength and fracture toughness. Investigating crack interactions helps engineers and researchers identify potential failure mechanisms,

develop effective mitigation strategies, and enhance the durability and safety of engineering components. Bisht et al. (2015) used Finite element method to analyze multiple crack interactions in a rectangular plate, revealing intensification and shielding effects with crack offset distance and non-desirability of close crack proximity for structural integrity. Vivekanandan & Ramesh (2020) investigated the impact of interacting internal cracks on edge cracks in a transient thermal stress field using digital photo-thermoelastic experiments and finite element analysis. Mishra et al. (2019) studied the behaviour of piezoelectric components with multiple cracks under thermo-electro-mechanical loading using the extended finite element method and decoupled thermo-electro-elastic problems, predicting stress intensity factors. Pathak (2020) analysed the interaction of multiple cracks in functionally graded materials (FGMs) under mixed mode mechanical and thermal loading, using extrinsically enriched Extended Finite Element (XFEM) approach to model crack discontinuities and exponential law to represent the heterogeneous material property. Mishael et al. (2023) proposed a general methodology for numerically simulating stress intensity factor (SIF) and crack growth in marine structures, considering interaction effects and crack coalescence, and provided insights for fatigue analysis of offshore wind structural components. The literature reveals the use of different analytical and computational tools in analysing the effect of crack in components. The most common computational methods are finite element method, finite difference method, boundary element method etc. Over time, numerous methodologies have been devised within Finite Element Method (FEM) (Yaghi & Becker, 2004) to examine stress distribution at the crack tip. Nonetheless, in FEM, a crack must align with the boundaries of finite elements, which entails utilizing a conformal mesh and specialized elements to account for asymptotic stress field at crack tip. Consequently, the process of modelling and simulating discontinuities and defects using FEM becomes intricate and burdensome. Continuous advancements in these mesh-based methods led to the evolution of various mesh-free methods. Various computational methods like Extended finite element method, and other meshfree methods have recently gained some significance is the crack interaction problems. Mesh-free methods rely only on nodal points for constructing approximations, which effectively eliminates the drawbacks inherent in mesh-based methods. Out of these Element free Galerkin method (EFGM) (Belytschko et al., 1994) has contributed most to the simulation of fracture problems (Zhang et al., 2019; Kumar & Ghosh, 2021). EFGM stands out among other mesh-free techniques employed in fracture problems due to its ability to eliminate the need for re-meshing and redistribution of nodal data. In EFGM only nodal data is required and discretizes the domain by inserting the gauss points of some order in between the nodes for the interpolation. The nodal approximation is achieved through the Moving Least Squares (MLS) method, while numerical integration is conducted by establishing a simplified "mesh" of rectangular cells. These cells are used to define integration points and their corresponding weights. The concept of nodal influence domain is utilized to obtain the shape functions and derive the nodal stiffness matrix. Since EFGM has emerged as a significant tool in the application of fracture problems, Subsequent attention has been directed towards refining and enhancing its capabilities to increase flexibility and efficiency beyond its conventional form (Garg & Pant, 2018a; Awasthi & Pant, 2022). This enhancement can be in the form of computational accuracy or versatility in dealing with complex problems. The novelty of current study lies in the exploration of crack interaction studies using the Element free Galerkin method (EFGM) under thermomechanical loading conditions which have not been significantly explored. Modification in the existing intrinsic enrichment for crack interaction study has also been proposed for accurately modelling and evaluating the crack interaction effect. Moreover, the implementation of EFGM for crack interaction study in diverse materials also adds to the worth of proposed work.

Paper has been organized in six sections. First part highlights the introduction of different approaches for handling crack interaction problems. In the second section basic introduction of Element free Galerkin method have been presented for providing insights for modelling of different kind of materials. Section three discusses the Interaction integral required in evaluation for stress intensity factors for different kind

of materials. In section four the newly proposed modified intrinsic enrichment has been proposed. In section five, one benchmark problem has been simulated to present the efficiency of proposed criterion along with other crack interaction problems in thermoelastic loadings in different kind of materials. Last two sections comprise of conclusions drawn from present study followed by references.

2. Element Free Galerkin Method Formulation

The evaluation of field variables in EFGM is based on Moving least square (MLS) approximations. MLS was initially developed by Ouhainou et al. (2010), Lancaster & Salkauskas (1981) for data interpolation. Their idea was subsequently implemented in EFGM for the evaluation of the field variable $u^h(x)$ given by the relation:

$$u^h(x) = \sum_{j=1}^m p_j(x) a_j(x) = p^T(x) a(x) \quad (1)$$

Here $p^T(x)$ is complete basis function vector and $a(x)$ represents vector of undetermined coefficients given as given as (Pant et al., 2010):

$$p^T(x) = [1, x, y, xy, x^2, y^2, \dots \dots x^{k'}, y^{k'}] \quad (2)$$

$$a^T(x) = [a_1(x), a_2(x) \dots \dots a_n(x)] \quad (3)$$

Value of shape function is determined by evaluating $a(x)$, which is calculated for any point x , Quadratic form of weighted least square sum ($L(x)$) is given as (Pant et al., 2011b):

$$L(x) = \sum_{I=1}^n w(x - x_I) [p^T(x) a(x) - u_I]^2 \quad (4)$$

Here, $w(x - x_I)$ is represents weight function associated to node I , having n number of nodes inside influence domain linked to point (x) . After implementing minimization using $\delta L / \delta a = 0$, leads to the equation as (Pant et al., 2011b):

$$A(x) a(x) = B(x) u \quad (5)$$

where,

$$A(x) = \sum_{I=1}^n w(x - x_I) p(x_I) p^T(x_I) \quad (6)$$

$$B(x) = \{w(x - x_1) p(x_1), (x - x_2) p(x_2), (x - x_3) p(x_3) \dots \dots (x - x_n) p(x_n)\} \quad (7)$$

Now substituting the value of $a(x)$ from eq. (5) in the eq. (1), approximation function obtained is given as:

$$u^h(x) = \sum_{I=1}^n \varphi_I(x) u_I \quad (8)$$

Here φ_I is the meshfree shape function, given by the relation as:

$$\varphi_I(x) = \sum_{j=1}^m p_j(x) (A^{-1}(x) B(x))_{jI} = p^T A^{-1} B_I \quad (9)$$

In this MLS approximation choice of weight function ($w(x - x_I)$) greatly effects the accuracy of approximation. Its continuity and smoothness are directly linked with continuity and smoothness of shape function ($\varphi_I(x)$). Expression of cubic spline weight function taken in current study is given as (Singh, 2005):

$$w(x - x_I) = \begin{pmatrix} 4r^3 - 4r^2 + 2/3 & r \leq (1/2) \\ -4r^3/3 + 4r^2 - 4r + 4/3 & (1/2) < r \leq 1 \\ 0 & r > 1 \end{pmatrix} \quad (10)$$

Here, $r = \frac{|x-x_I|}{d_{mI}}$ where $(x - x_I)$ is distance between node (x_I) and evaluation point x , d_{mI} is domain of influence of node (x_I) . Consider a 2D FGM domain bounded by Γ , under the action of various forces as shown in Figure 1. Here \bar{u} is displacement vector and \bar{t} is traction force.

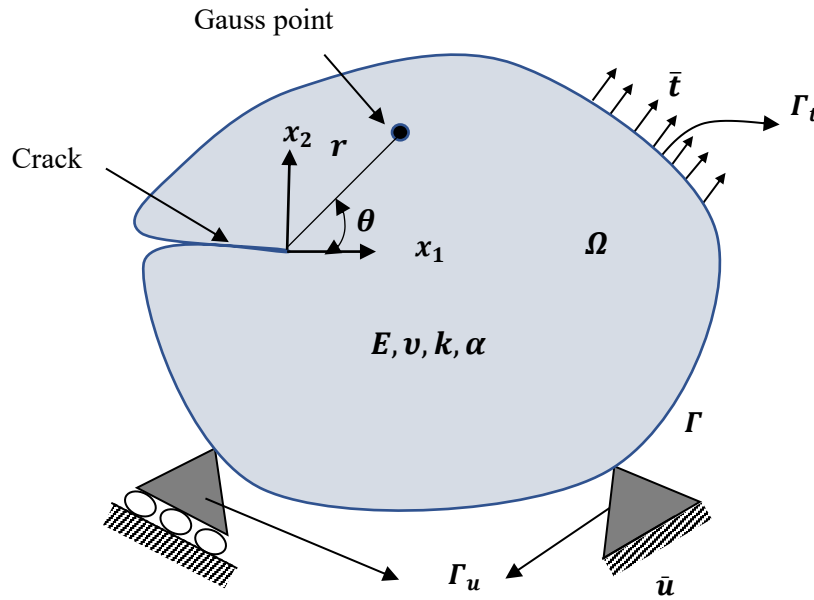


Figure 1. Domain representation with boundary conditions.

Governing equation of equilibrium for linear thermoelastic problems is given by relation (Pant et al., 2011b):

$$\nabla \cdot \sigma + b = 0 \text{ in } \Omega \tag{11}$$

$$-\nabla q + Q = 0 \text{ with } q = -k\nabla T \tag{12}$$

Here, σ is stress tensor, ϵ is strain tensor, b is body force vector, Q is heat source, q is heat flux vector, u is displacement vector, α is thermal expansion coefficient.

$$\sigma = D (\epsilon_{mechanical} - \epsilon_{thermal}), \quad \epsilon_{mechanical} = \nabla_S u, \quad \epsilon_{thermal} = \alpha(T - T_0)I \tag{13}$$

Here, D is material constant matrix. D matrix for different types of materials under plane stress condition is given as:

(i) Isotropic material

$$D = \left(\frac{E}{1-\nu} \right) \begin{bmatrix} 1 & \nu & 0 \\ \nu & 1 & 0 \\ 0 & 0 & \frac{(1-\nu)}{2} \end{bmatrix} \tag{14}$$

where, E is young's modulus and ν is poisons ratio.

(ii) Functionally graded material

$$E = E(x) = E(x_1, x_2), \nu = \nu(x) = \nu(x_1, x_2)$$

$$\mathbf{D}(x) = \frac{E(x)}{(1 - \nu(x)^2)} \begin{bmatrix} 1 & \nu(x) & 0 \\ \nu(x) & 1 & 0 \\ 0 & 0 & \frac{(1 - \nu(x))}{2} \end{bmatrix} \quad (15)$$

Here (x) signify the geometry parameter for variable properties at different locations in the domain.

(iii) Orthotropic material

$$\mathbf{D} = \begin{bmatrix} \frac{1}{E_1} & -\frac{\nu_{12}}{E_1} & 0 \\ -\frac{\nu_{12}}{E_1} & \frac{1}{E_2} & 0 \\ 0 & 0 & \frac{1}{G_{12}} \end{bmatrix} \quad (16)$$

(iv) Bimaterial

$$\mathbf{D}_i = \left(\frac{E_i}{1 - \nu_i} \right) \begin{bmatrix} 1 & \nu_i & 0 \\ \nu_i & 1 & 0 \\ 0 & 0 & \frac{(1 - \nu_i)}{2} \end{bmatrix} \quad (17)$$

Here i signify the number of materials in the bimaterial, each having its own material properties. Lagrange multiplier approach have been used to enforce essential boundary conditions depending upon the type domain. So, discrete equations have been obtained as (Pant et al., 2011a):

$$\begin{bmatrix} K & G \\ G^T & 0 \end{bmatrix} \begin{bmatrix} T \\ \lambda \end{bmatrix} = \begin{bmatrix} f_I \\ R_k \end{bmatrix} \quad (18)$$

$$\text{where, } K_{IJ} = \int_{\Omega} \begin{bmatrix} \varphi_{I,x} & 0 \\ \varphi_{J,y} & k_y \end{bmatrix} \begin{bmatrix} k_x \\ \varphi_{J,y} \end{bmatrix} d\Omega, \quad f_I = \int_{\Omega} Q \varphi_I d\Omega, \quad G_{IK} = \int_{\Gamma_T} \varphi_I N_k d\Gamma \quad \text{and} \quad R_k = \int_{\Gamma_T} \bar{T} N_k d\Gamma.$$

and from Eq. (11) and Eq. (14). Discrete equations obtained are as follows:

$$\begin{bmatrix} K & G \\ G^T & 0 \end{bmatrix} \begin{bmatrix} u \\ \lambda \end{bmatrix} = \begin{bmatrix} f \\ R \end{bmatrix} \quad (19)$$

$$\text{where, } K_{IJ} = \int_{\Omega} B_I^T D B_J d\Omega, \quad f_I = \int_{\Omega} B_I^T D \epsilon_T d\Omega + \int_{\Omega} \bar{t} \varphi_I d\Gamma, \quad G_{IK} = - \int_{\Gamma_u} \varphi_I N_k d\Gamma \quad \text{and} \quad R_k = - \int_{\Gamma_u} \bar{T} N_k d\Gamma, \quad N_K = \begin{bmatrix} N_K & 0 \\ 0 & N_K \end{bmatrix}, \quad B_I = \begin{bmatrix} \varphi_{I,x} & 0 \\ 0 & \varphi_{I,y} \\ \varphi_{I,y} & \varphi_{I,x} \end{bmatrix}, \quad D \text{ is material constant matrix as specified in Equations (14-17).}$$

Crack is modelled in current work using the full intrinsic enrichment criteria. In this there is no physical crack present in domain, but presence of a crack is ensured by incorporating additional terms into the basis function, known as enrichment terms. The selection of these enrichment terms depends upon the level of accuracy required. A full or complete intrinsic enriched basis function for linear elastic fracture mechanics problems can be given as (Pant et al., 2011a):

$$P^E(x) = \left[1 \quad x \quad y \quad \sqrt{r} \sin \frac{\theta}{2} \quad \sqrt{r} \cos \frac{\theta}{2} \quad \sqrt{r} \sin \frac{\theta}{2} \sin \theta \quad \sqrt{r} \cos \frac{\theta}{2} \sin \theta \right] \quad (20)$$

Here r and θ are crack tip parameters as shown in Figure 1. First three terms of enriched basis function ($P^E(x)$) are linear basis functions and remaining trigonometric functions are enrichment terms. Number of terms in the enriched basis function decides the accuracy of approximation but this increases size of stiffness matrix so its inversion becomes quite cumbersome.

3. J -Integral Formulations for Different Materials

The interaction integrals employed for computing stress intensity factors for different types of materials are briefly discussed as follows:

(i) Interaction integral for isotropic materials under mechanical loading (Pant et al., 2010):

$$M^{(1,2)} = \int_A \left[\sigma_{ij}^{(1)} \frac{\partial u_i^{(2)}}{\partial x_1} + \sigma_{ij}^{(2)} \frac{\partial u_i^{(1)}}{\partial x_1} - W^U \delta_{ij} \right] \frac{\partial q}{\partial x_j} dA \quad (21)$$

(ii) Thermal interaction integral for isotropic materials under thermal loading (Pant et al., 2010):

$$M^{(1,2)} = \int_A \left[\sigma_{ij}^{(1)} \frac{\partial u_i^{(2)}}{\partial x_1} + \sigma_{ij}^{(2)} \frac{\partial u_i^{(1)}}{\partial x_1} - W^U \delta_{ij} \right] \frac{\partial q}{\partial x_j} dA + \alpha \int_A \frac{\partial T}{\partial x_1} \sigma_{kk}^2 q dA \quad (22)$$

Here, T is Temperature applied, α is coefficient of thermal expansion and σ_{kk} is thermal stress.

(iii) Thermal interaction integral for orthotropic materials under the thermal loading (Jia et al., 2015):

$$M^{(1,2)} = \int_A \left[\left(\sigma_{ij}^{(1)} \frac{\partial u_i^{(2)}}{\partial x_1} + \sigma_{ij}^{(2)} \frac{\partial u_i^{(1)}}{\partial x_1} \right) - \frac{1}{2} \left(\sigma_{ij}^{(1)} \varepsilon_{ij}^{(2)} + \sigma_{ij}^{(2)} \varepsilon_{ij}^* \right) \delta_{1j} \right] \frac{\partial q}{\partial x_j} dA + \int_A \left[\sigma_{ij}^{(2)} \alpha_{ij}^{(1)} \frac{\partial T}{\partial x_1} \right] q dA \quad (23)$$

where, $\varepsilon_{ij}^* = \varepsilon_{ij}^{(1)} - \alpha_{ij}^{(1)} (T_1^{(1)} - T_0^{(1)})$, superscript 1 is for actual state and 2 for auxiliary state.

(iv) Thermal interaction integral for functionally graded media under the thermal loading (Bhardwaj et al., 2021):

$$M^{(1,2)} = \int_A \left\{ \sigma_{ij}^{(1)} \frac{\partial u_i^{(2)}}{\partial x_1} + \sigma_{ij}^{(2)} \frac{\partial u_i^{(1)}}{\partial x_1} - \frac{1}{2} \left(\sigma_{ik}^{(1)} \varepsilon_{ik}^{(2)} + \sigma_{ik}^{(2)} \varepsilon_{ik}^{(1)} \right) \delta_{1j} \right\} \frac{\partial q}{\partial x_j} dA + \int_A \left\{ \frac{\partial \sigma_{ij}^{(2)}}{\partial x_j} - \varepsilon_{kl}^{(1)} \frac{\partial C_{ijkl}}{\partial x_1} \varepsilon_{ij}^{(2)} + \sigma_{ij}^{(2)} \left(\frac{\partial \beta}{\partial x_1} \Delta \theta + \alpha \frac{\Delta \theta}{\partial x_1} \right) \right\} q dA \quad (24)$$

where, $\alpha = \alpha(x)$ is thermal expansion coefficient and $\Delta \theta$ is temperature gradient.

(v) Thermal interaction integral for bimaterial under the thermal loading (Garg & Pant, 2018b):

$$M^{(1,2)} = \sum_{m=1}^2 \int_{A_m} \left[\sigma_{ij}^{(1)} \frac{\partial u_i^{(2)}}{\partial x_1} + \sigma_{ij}^{(2)} \frac{\partial u_i^{(1)}}{\partial x_1} - W^U \delta_{1j} \right] \frac{\partial q}{\partial x_j} dA + \sum_{m=1}^2 \alpha \int_{A_m} \frac{\partial T}{\partial x_1} \sigma_{kk}^{(2)} q dA \quad (25)$$

where, m is particular material in the bimaterial, q is weight function whose value is unity at tip of crack and zero on J integral contour.

4. Modified Intrinsic Enrichment

In conventional EFGM the formation of a Global stiffness matrix $[K]_{IJ}$ is solely dependent on the attributes of the primary crack. This leads to an inaccurate assessment of fields in case where multiple cracks are present in the domain. This makes the modelling of unequal cracks and their subsequent interactions difficult. When multiple cracks are present in the domain, the conventional EFGM utilizes the concept of minimum normalized distance which means the equation points gets the contribution from the nearest crack tip only in spite of presence of other cracks. Due to the inherent complexity of dealing with multiple cracks

of varying sizes and their interactions, the existing criterion encounters significant difficulty. To overcome such problems, this study introduces modifications to the current intrinsic enrichment criterion, enabling it to effectively accommodate multiple cracks of all sizes. So, a modification in the framework of EFGM in assembly of Global stiffness matrix has been presented to accurately evaluate the field variables in case of multiple cracks. Initial step of the current approach is evaluation of distances of evaluation point to all present crack tips. Distances are then normalized by corresponding crack lengths. The relative contributions of different crack tips within a domain are determined by their normalized distances from respective crack tips. So, according to the current criterion, each crack contributes to the formation of Global stiffness matrix $[K]_{JJ}$ at each evaluation point. The level of contribution is calculated from the normalized distances such that the crack tip near to Gauss point will have a higher contribution than the other cracks. Consider a plate having three cracks c_1 , c_2 and c_3 as shown in Figure 2.

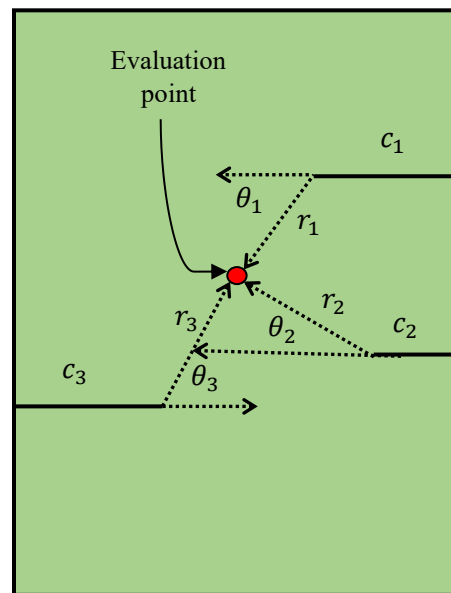


Figure 2. Crack tip parameters for three cracks in plate along with evaluation point.

Gauss points location with respect to different crack tips is given as: $(c_1, \theta_1), (c_2, \theta_2), (c_3, \theta_3)$. Now for each evaluation point, the distance is calculated from each crack tip as: r_1, r_2, r_3 . These distances are normalized by the consecutive cracks lengths as: $d_1 = \frac{r_1}{c_1}, d_2 = \frac{r_2}{c_2}, d_3 = \frac{r_3}{c_3}$. Now the contribution factor (R) is calculated as: $s_1 = d_1^C, s_2 = d_2^C, s_3 = d_3^C$, here C is the predefined constant whose value is evaluated using sensitivity analysis and its acceptable value has found to be from -50 to -100. Now, $s = s_1 + s_2 + s_3$. Now Contribution factor corresponding to each crack tip is given as: $R_1 = s_1/s, R_2 = s_2/s$ and $R_3 = 1 - R_1 - R_2$. So corresponding global stiffness gets modified as:

$$[K]_{total} = [K]_1 \times R_1 + [K]_2 \times R_2 + [K]_3 \times R_3 \quad (26)$$

For N number of cracks Eq. (26) gets modified as:

$$[K]_{total} = [K]_1 \times R_1 + [K]_2 \times R_2 + \dots + [K]_N \times R_N = \sum_{k=1}^N [K]_k \times R_k \quad (27)$$

The proposed criterion takes into account the influence of all cracks at every evaluation point within the domain. As a result, it can be effortlessly applied to analyse scenarios involving multiple cracks, involving different lengths and orientations.

5. Results and Discussions

5.1 Isotropic Plate under Mechanical Loading

In the current study a rectangular plate having dimensions $W = 100 \text{ cm}$, $H = 200 \text{ cm}$ having multiple cracks is considered. The material selected for present study is taken as ASTM 36 steel having properties (Beer, 2011; Bhardwaj et al., 2021): Young's modulus (E) = 200 GPa , Poisson's ratio (ν) = 0.3 Coefficient of thermal expansion (α) = $11.7 \times 10^{-6} \text{ K}^{-1}$. The plate is having three cracks such that the first crack ($a_1 = 50 \text{ mm}$) is on the left edge of the plate, second crack ($a_2 = 40 \text{ mm}$) is located at a distance of 115 cm from the bottom edge in the right side of plate. The third crack ($a_3 = 40 \text{ mm}$) is located at 85 cm from bottom edge in the right side of the plate. First and second crack are oriented horizontally while the third crack is inclined at angle 30° to horizontal as shown in Figure 3. Domain has been discretized by taking of 800 (20×40) nodes. Far field stress field of 100 MPa is applied at the top edge of plate. Boundary conditions have been shown in Figure 3. Mode I and Mode II Stress intensity factor at the left crack tip with variation in crack orientation of third crack have been evaluated. Stress intensity factor have been calculated using Eq. (21) following similar methodology to reference (Pant et al., 2010). Figure 4 (a) and Figure 4 (b) shows comparison of σ_{yy} stress fields evaluated using the conventional EFGM and proposed modified enrichment respectively. From Figure 4 it can be clearly seen that modified enrichment gives better stress fields in comparison to conventional EFGM for interacting cracks. Variation of Mode I and Mode II stress intensity factor for left crack tip with variation in crack orientation of second crack (a_2) have been shown in Figure 5. Mode I SIF initially increased and then decreased with the with an increase in crack angle as shown in Figure 5 (a). While value of Mode II SIF initially decreased and then increased with an increase in crack angle as shown in Figure 5 (b). Results clearly indicate that the orientation of secondary crack has significant influence in stress intensity factor at the left crack tip.

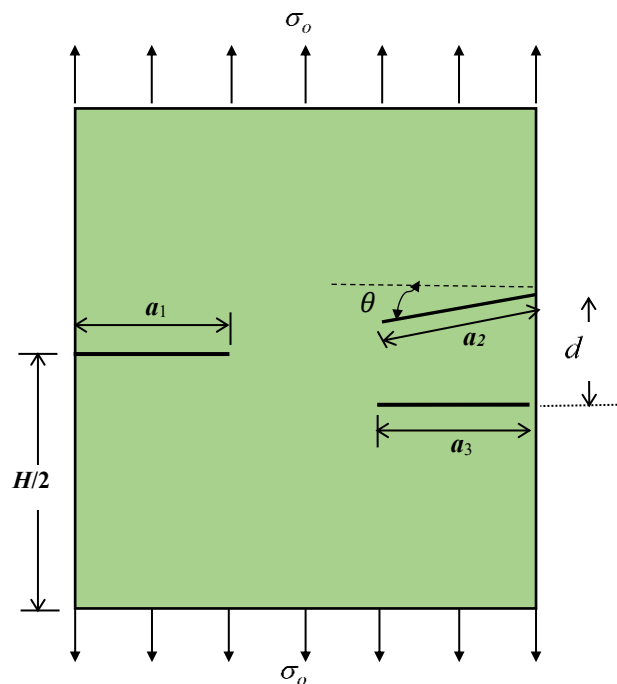


Figure 3. Crack tip parameters for three cracks in plate along with evaluation point.

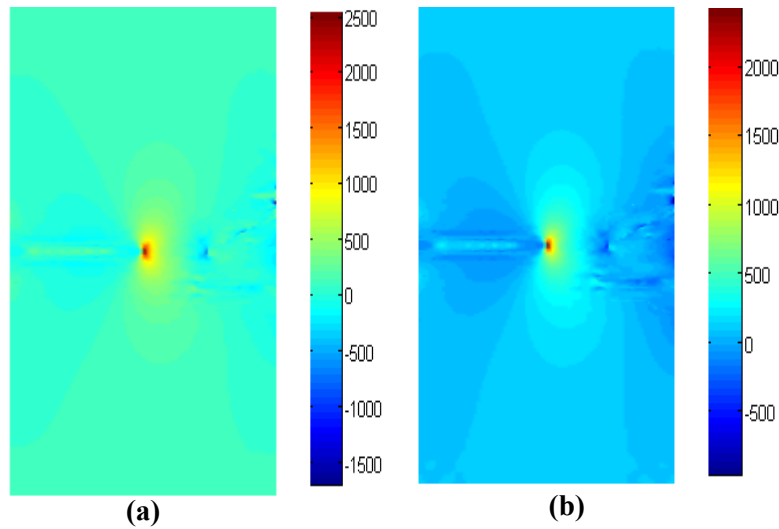


Figure 4. σ_{yy} profile (a) Conventional intrinsic enrichment (b) Modified intrinsic enrichment.

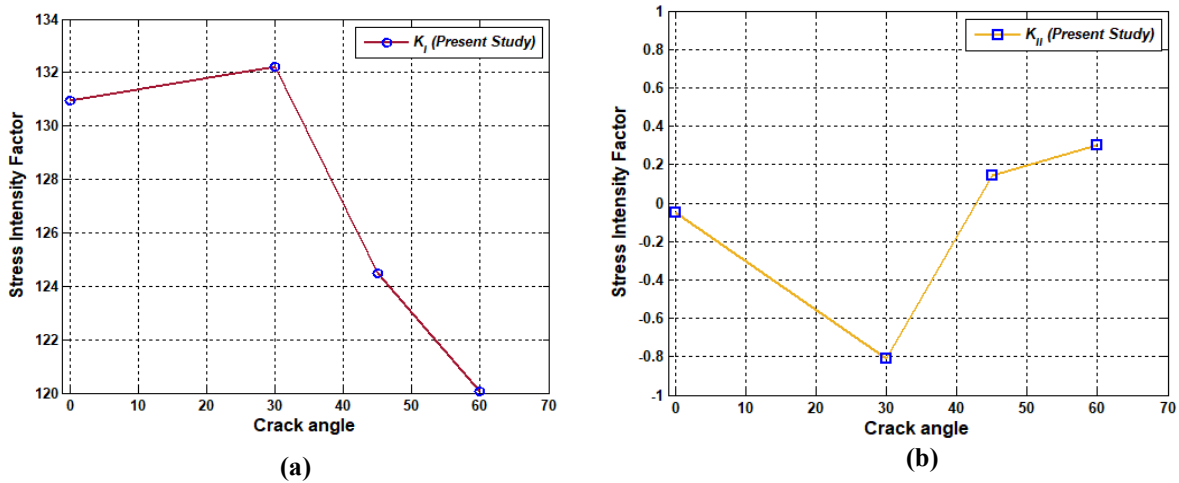


Figure 5. Variation of SIF ($MPa\sqrt{m}$) at left-tip with crack angle (second crack) (a) Mode I (b) Mode II.

5.2 Isotropic Plate under Thermal Loading

A rectangular plate having multiple cracks subjected to thermoelastic loading have been considered in current problem. Dimensions of plate are as: $W = 100\text{ cm}$, $H = 200\text{ cm}$, Major crack length (A) = 20 cm , Initial minor crack length (a) = 10 cm . The material selected for present study is taken as ASTM 36 steel having properties (Beer, 2011): Youngs modulus (E) = 200 GPa , Poisson's ratio (ν) = 0.3 . Coefficient of thermal expansion (α) = $11.7 \times 10^{-6} K^{-1}$. Thermal boundary conditions include temperature of -50°C on the top edge, 50°C on the bottom edge and thermal insulation on the remaining edges. Mechanical constraints along with boundary conditions have been shown in Figure 6 (a). Discretization of domain have been done by taking 20 nodes in x-direction and 40 nodes in y-direction that is total of 800 nodes. Temperature difference between the top and bottom edge of plate causes the generation

of heat flux in the domain. Since both the cracks lie across the range of heat flux so they generate discontinuity in thermal fields which can be clearly seen from Figure 6 (b) and (c). Obtained thermal fields are used as an input in evaluation of stresses and eventually evaluating stress intensity factors. Variation of Mode I and Mode II Stress intensity factor at the left crack tip with an increase in crack increment of right crack have been shown in Figure 7. Stress intensity factor (SIF) have been calculated using Eq. (22) following similar methodology to reference (Pant et al., 2010). Mode II SIF for the left crack increased with crack increment of right crack up to 0.2m or 20cm which declined afterwards whereas no significant change in Mode I SIF with respect to crack increment was observed.

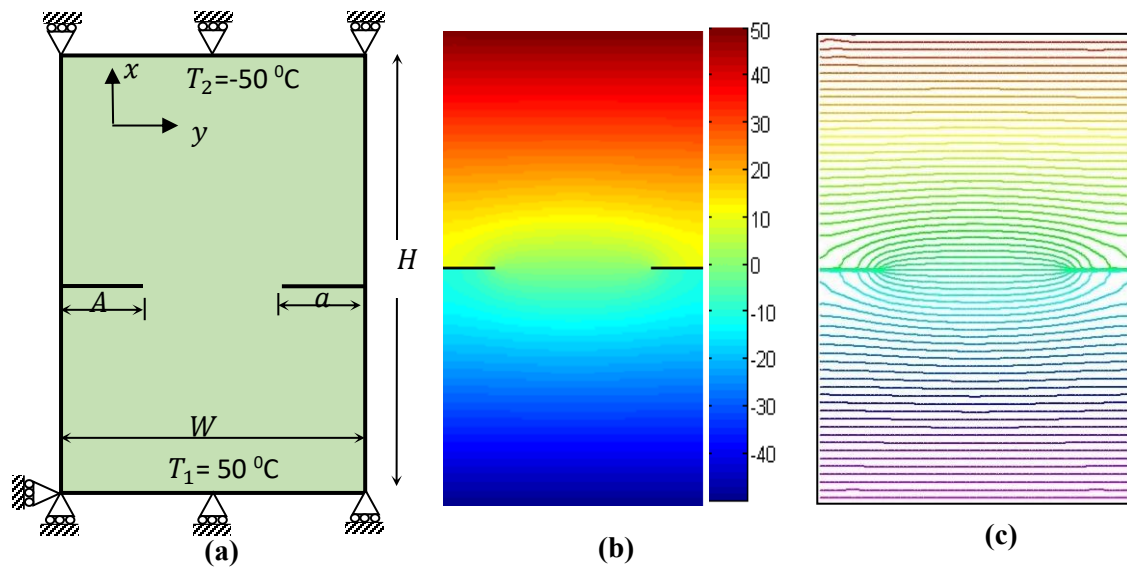


Figure 6. (a) Problem geometry with boundary conditions (b) Temperature profile (c) Thermal contours.

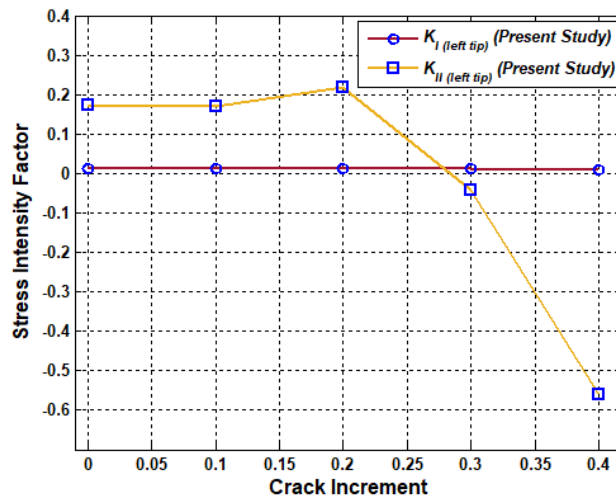


Figure 7. Variation of Mode I and Mode II SIF ($MPa\sqrt{m}$) at left crack tip with crack increment (m) of right crack.

5.3 Orthotropic Plate under Thermal Loading

In the current problem crack interaction in orthotropic media under thermal loading have been studied. Dimensions of plate along with boundary conditions have been shown in Figure 8 (a). The material selected for present study is taken as orthotropic Glass/Epoxy having properties (Pasternak, 2012): $E_1 = 55 \text{ GPa}$, $E_2 = 21 \text{ GPa}$, $G_{12} = 9.7 \text{ GPa}$, $\nu_{12} = 0.25$ $\alpha_{11} = 6.3 \times 10^{-6} \text{ K}^{-1}$, $\alpha_{22} = 2 \times 10^{-5} \text{ K}^{-1}$, $k_{11}/k_{11} = 3.46/0.35$. Cracks has been modelled as an isothermal boundary where they are maintained at a temperature of 0°C . All edges of plate are placed at the temperature of 10°C . Discretization of domain involves taking total of 800 nodes (20×40). Continuous temperature fields have been observed around crack surface which is a property of isothermal boundary as shown in Figure 8 (b) and (c). Mode I and Mode II Stress intensity factor for right tip of the lower crack have been evaluated using Eq. (23) following similar methodology to reference (Jia et al., 2015). Stress intensity factor is normalised by $10 \times E_2 \alpha_{22} \sqrt{\pi a}$. Various of distance between both the cracks along with the crack length have been evaluated and compared with reference results (Pasternak, 2012) as shown in Figure 9 (a) and (b).

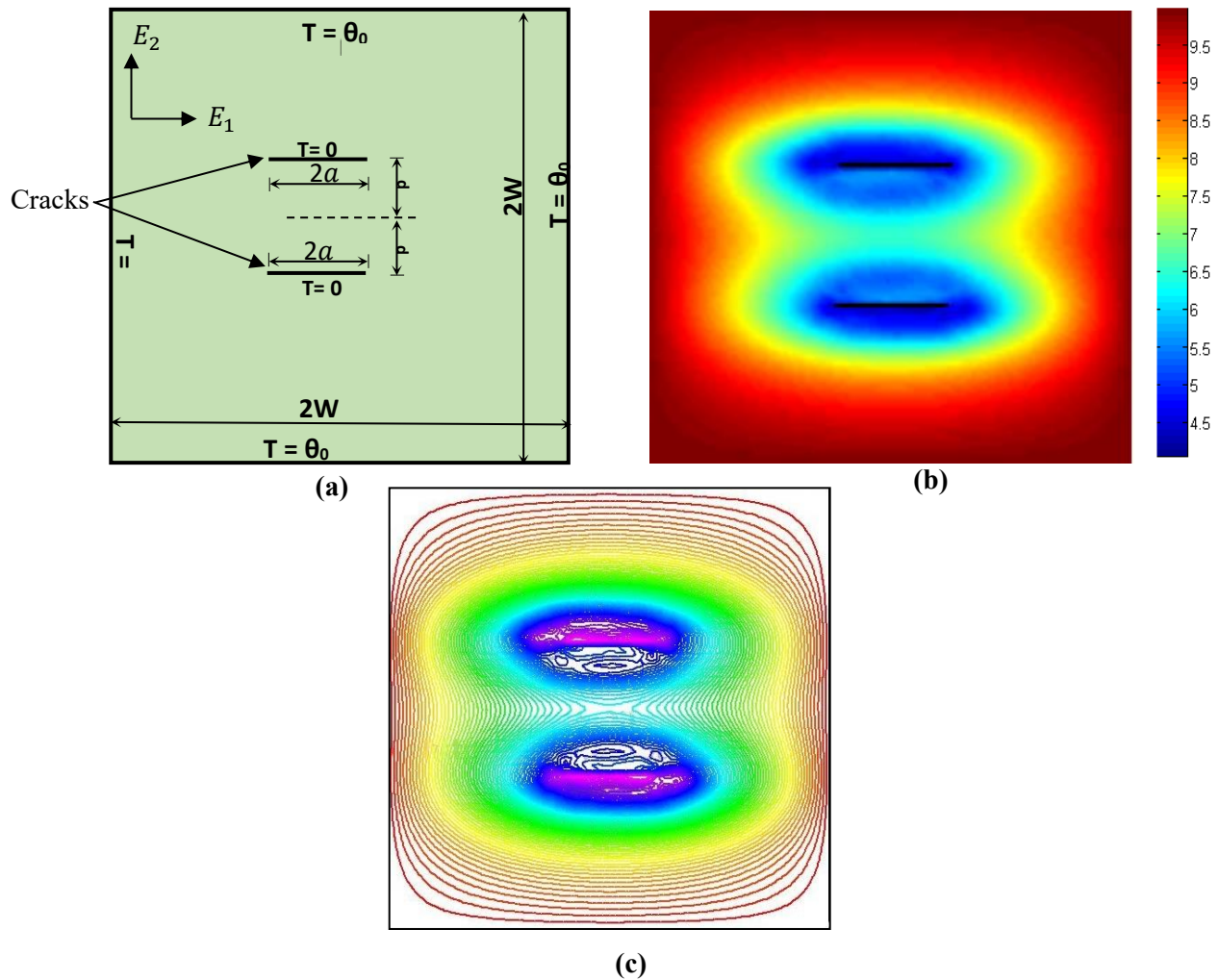


Figure 8. (a) Problem geometry with boundary conditions (b) Temperature profile (c) Thermal contour.

Obtained results have been in good agreement with the reference results. Values of Mode I SIF initially increased with the increase in d/W ratio and finally decreased, whereas Mode II SIF gets varied in its reverse manner. This indicates that the distance between two cracks and crack length are the major parameter influencing the stress intensity factors.

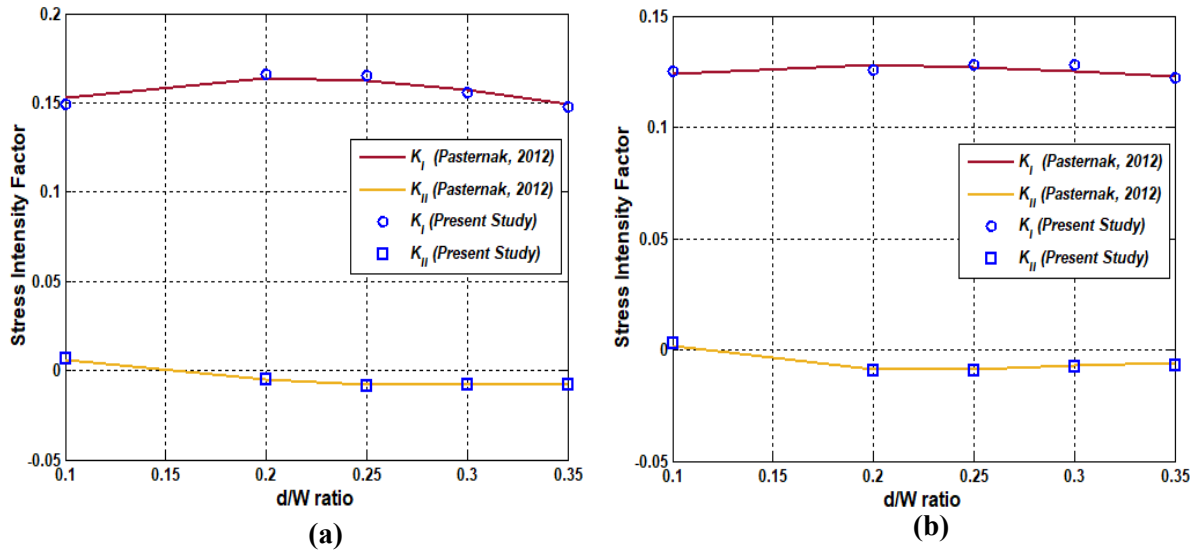


Figure 9. Variation of mode I and mode II SIF ($MPa\sqrt{m}$) for right tip of the lower crack with d/W ratio (a) $a/W = 0.3$ (b) $a/W = 0.5$.

5.4 Functionally Graded Plate under Thermal Loadings

In the current problem multiple crack interaction under thermal loading have been studied. Dimensions of functionally graded plate along with boundary conditions have been shown in the Figure 10 (a). Rectangular plate ($100mm \times 200mm$) consists of two edge cracks ($a = 20mm$) on right edge and left edge respectively, along with one inclined centre crack ($A = 30mm$) in between them. Thermal boundary conditions include $20^\circ C$ on left edge and $200^\circ C$ on right edge. Top and bottom edges have been kept insulated. Left and right edges of plate have been mechanically constraint for displacement in horizontal direction. Bottom left corner node is restrained in both horizontal and vertical direction. Discretization in current problem is done by taking 800 nodes (20×40). FGM plate considered in current example consists of aluminium alloy on left side which grades towards ceramic on right side. Material properties of this FGM plate are given in Table 1 and are varied as follows:

$$E(x) = E_{aluminium} e^{\alpha x}, \text{ where } \alpha = (1/L) \times \ln(E_{ceramic}/E_{aluminium}) \tag{28}$$

$$V_{ceramic}(x) = \frac{E(x) - E_{aluminium}}{E_{ceramic} - E_{aluminium}} \tag{29}$$

$$V_{aluminium} = 1 - V_{ceramic}(x) \tag{30}$$

$$\nu(x) = \frac{(v_{aluminium} \times V_{aluminium}(x) \times E_{ceramic}) + (v_{ceramic} \times (x) \times E_{aluminium})}{(V_{aluminium}(x) \times E_{ceramic}) + \dots} \tag{31}$$

$$\alpha(x) = \alpha_{aluminium} e^{\Psi x} \text{ where } \Psi = (1/L) \times \ln(\alpha_{ceramic}/\alpha_{aluminium}) \quad (32)$$

$$k(x) = \alpha_{aluminium} e^{\delta x} \text{ where } \delta = (1/L) \times \ln(k_{ceramic}/k_{aluminium}) \quad (33)$$

Here E is Young's modulus, V is volume fraction, ν is Poisson's ratio, α is coefficient of thermal expansion and k is thermal conductivity.

Table 1. Material properties of constituents of FGM (Pathak, 2020).

Material	E (GPa)	ν	$\alpha * 10^{-6} \text{ } ^\circ\text{C}^{-1}$	K (W/m $^\circ\text{C}$)
Alloy	70	0.3	25	200
Ceramic	360	0.25	8.2	30

Clear discontinuity in thermal fields is observed across Inclined centre crack as clearly seen from Figure 10 (b) and (c). However, no discontinuity in thermal fields is observed around the edge cracks as they are parallel to the heat flux. Crack across the thermal heat flux in acting as a barrier for heat transfer whereas crack along it does not affect the thermal heat flux. Obtained thermal fields are then used as an input in evaluating stresses and eventually Stress intensity factors. Mode I and Mode II stress intensity factors for the centre crack for both tips with variation in its orientation have been evaluated in the present study. Stress intensity factor (SIF) have been calculated using Eq. (24) following similar methodology to reference (Pathak, 2020). Stress intensity factors obtained at both tips have been compared with reference results (Pathak, 2020). Obtained results have been in good agreement with the reference results as clearly seen from Figure 11 (a) and (b). For the left tip, the values of both Mode I and Mode II SIF decreased with an increase in crack angle whereas for the right tips the values of SIF initially increased and then decreased.

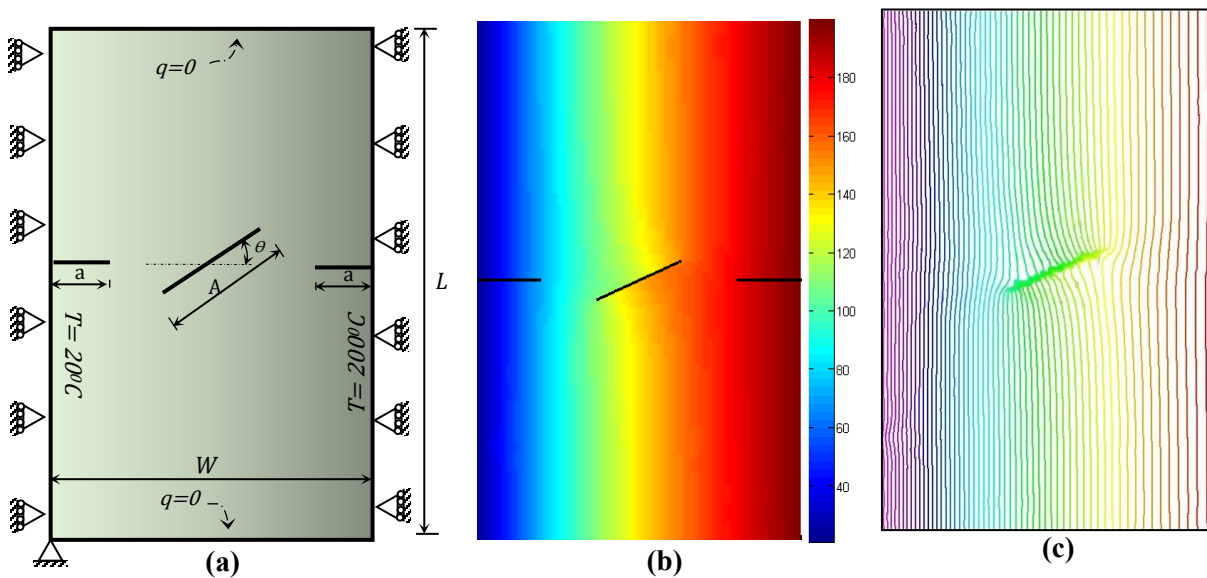


Figure 10. (a) Problem geometry with boundary conditions (b) Temperature profile (c) Thermal contours.

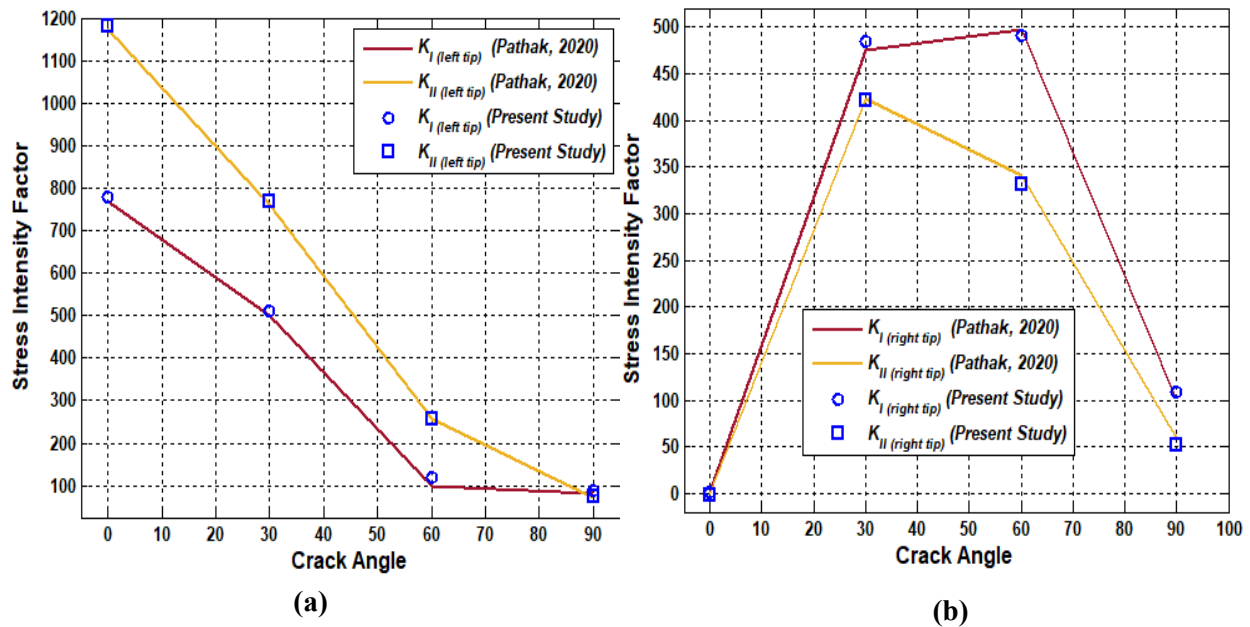


Figure 11. Variation of mode I and mode II SIF ($MPa\sqrt{m}$) for center crack with its crack orientation angle (a) Left tip (b) Right tip.

5.5 Bimaterial Plate under Thermal Loading

In the current problem multiple crack interaction in bimaterial rectangular plate under thermal loading have been studied. Bimaterial plate ($203.2\text{ mm} \times 152.4\text{ mm}$) consists of one interfacial crack ($a = 20\text{ mm}$) and sub interfacial crack ($c = 20\text{ mm}$) which are placed such that longitudinal distance (d) between two cracks is 0 mm and vertical distance between the two is 2.5 mm as shown in Figure 12 (a). Thermal boundary conditions are: 200°C on the top edge, -200°C on the bottom edge, right and left edges are kept insulated for any heat transfer. Crack has been modelled as an adiabatic boundary. Bimaterial constitutes of S45C in upper region and Si_3N_4 on the lower region. Properties of bimaterial are given as: (Ouinias et al., 2010) $E_{\text{Si}_3\text{N}_4} = 206\text{ GPa}$, $E_{\text{S45C}} = 304\text{ GPa}$, $\nu_{\text{Si}_3\text{N}_4} = 0.30$, $\nu_{\text{S45C}} = 0.27$, $\alpha_{\text{Si}_3\text{N}_4} = 12 \times 10^{-6}$, $\alpha_{\text{S45C}} = 3 \times 10^{-6}$, $k_{\text{Si}_3\text{N}_4} = 42.7\text{ W/mk}^{-1}$, $k_{\text{S45C}} = 43\text{ W/mk}^{-1}$. Where E is Youngs modulus, ν is poissons ratio, α is coefficient of thermal expansion and k is thermal conductivity of the respective materials.

Bimaterial plate has been discretised by total of 800 nodes. Both interfacial and sub-interfacial cracks are across the direction of heat flux which generates discontinuity in thermal fields as clearly seen from Figure 12 (b) and (c). These fields are utilized for evaluation of thermal stress. Values of mode I and mode II stress intensity factor at interface edge crack (a) have been evaluated for variation of vertical distance (h) with respect to sub interfacial crack. Stress intensity factor (SIF) have been calculated using Eq. (25) following similar methodology to reference (Garg & Pant, 2018b). These results have been presented in Figure 13. Mode I Stress intensity factor showed irregular pattern however Mode II stress intensity factor decreased with an increase in offset distance between the cracks. This indicates that position of subterface crack significantly influences the SIF of the primary interfacial crack.

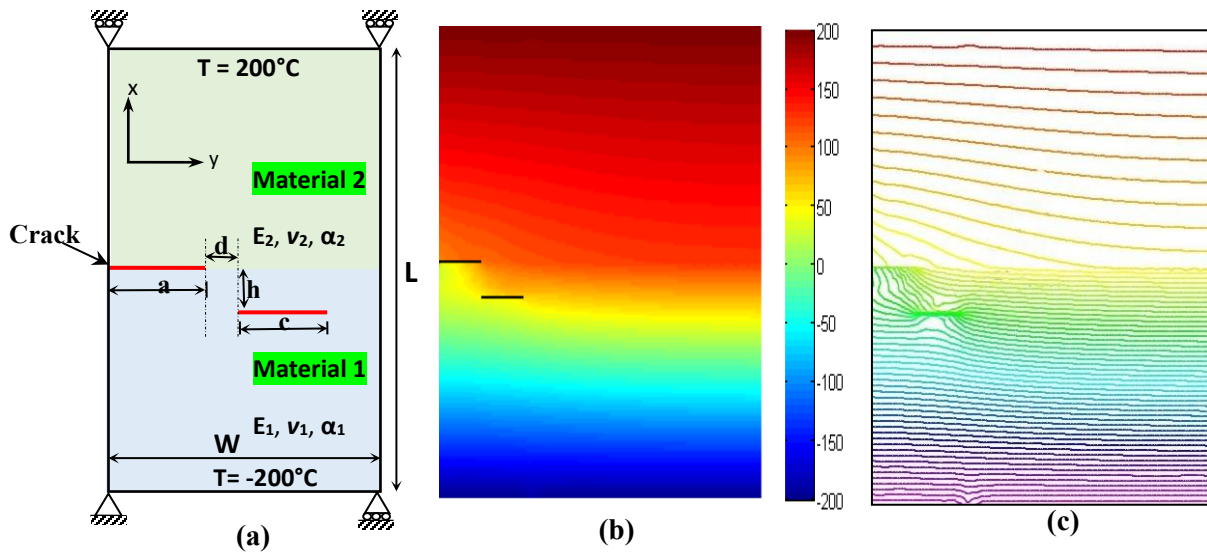


Figure 12. (a) Problem geometry with boundary conditions (b) Temperature profile (c) Thermal contours.

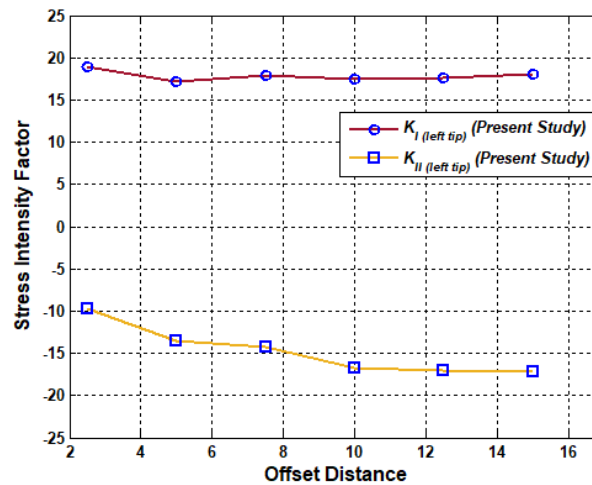


Figure 13. Variation of mode I and mode II SIF ($MPa\sqrt{m}$) for interface edge crack with offset distance(mm).

6. Conclusions

Study focused on the analysis of multiple cracks in various types of materials subjected to thermoelastic loadings using Element Free Galerkin method. Different kinds of materials like isotropic material, orthotropic material, functionally material graded and bimetals have been subjected to thermoelastic loadings in presence of multiple cracks. Results show that crack interactions have significant effect on the stress intensity factors. Modified enrichment presented in current work is more versatile than conventional enrichment in case of crack interactions. Also, parameters like crack length, crack orientation, distance between cracks, domain properties have significant effect on the stress intensity factor of the primary crack. This study gives insight into the effects of crack interactions in different kind of media under thermoelastic loadings. Thereby ensuring the structural integrity and durability of such materials for practical applications.

This enhanced EFGM algorithm's effectiveness can be expanded to address crack interactions in complex 3D fracture problems involving intricate shapes and different types of loadings.

Conflict of Interest

Authors have no conflict of interest to declare.

Acknowledgements

The Authors deeply acknowledges the computational facilities provided by Science and Engineering Research Board (SERB), Department of Science and Technology, Govt. of India under the research Grant No. ECR/2017/00013.

References

- Awasthi, A., & Pant, M. (2022). A revamped element-free Galerkin algorithm for accelerated simulation of fracture and fatigue problems in two-dimensional domains. *Iranian Journal of Science and Technology, Transactions of Mechanical Engineering*, 46(4), 1079-1106. <https://doi.org/10.1007/s40997-021-00471-z>.
- Awasthi, A., Panwar, N., Pant, M., Bala, S., Sharma, M.D., & Chauhan, A. (2021). Characterization, fabrication and dry sliding wear analysis of hybrid aluminium 6061 composite. *Tribology in Industry*, 43(4), 643-653. <https://doi.org/10.24874/ti.1012.11.20.03>.
- Beer, F.P. (2011). *Mechanics of materials* (Vol. 6). McGraw-Hill. India.
- Belytschko, T., Lu, Y.Y., & Gu, L. (1994). Element-free Galerkin methods. *International Journal for Numerical Methods in Engineering*, 37(2), 229-256. <https://doi.org/10.1002/nme.1620370205>.
- Bhardwaj, G., Singh, S.K., Patil, R.U., Godara, R.K., & Khanna, K. (2021). Thermo-elastic analysis of cracked functionally graded materials using XIGA. *Theoretical and Applied Fracture Mechanics*, 114, 103016. <https://doi.org/10.1016/j.tafmec.2021.103016>.
- Bisht, N., Gope, P.C., & Panwar, K. (2015). Influence of crack offset distance on the interaction of multiple cracks on the same side in a rectangular plate. *Frattura ed Integrità Strutturale*, 9(32), 1-12. <https://doi.org/10.3221/igf-esis.32.01>.
- Garg, S., & Pant, M. (2018a). Accelerated element-free Galerkin method for analysis of fracture problems. *Journal of the Brazilian Society of Mechanical Sciences and Engineering*, 40, 541. <https://doi.org/10.1007/s40430-018-1459-z>.
- Garg, S., & Pant, M. (2018b). Numerical simulation of thermal fracture in coatings using element free Galerkin method. *Indian Journal of Engineering and Materials Sciences*, 25(3), 217-232.
- Jia, H., Nie, Y., & Li, J. (2015). Fracture analysis in orthotropic thermoelasticity using extended finite element method. *Advances in Applied Mathematics and Mechanics*, 7(6), 780-795.
- Kolednik, O., Predan, J., & Fischer, F.D. (2010). Cracks in inhomogeneous materials: Comprehensive assessment using the configurational forces concept. *Engineering Fracture Mechanics*, 77(14), 2698-2711.
- Kumar, A., & Ghosh, R. (2021). Particularly optimized enriched element-free Galerkin method (POE-EFGM) for orthotropic fracture analysis of cortical bone. *Engineering Fracture Mechanics*, 254, 107943. <https://doi.org/10.1016/j.engfracmech.2021.107943>.
- Lancaster, P., & Salkauskas, K. (1981). Surfaces generated by moving least squares methods. *Mathematics of Computation*, 37(155), 141-158. <https://doi.org/10.1090/s0025-5718-1981-0616367-1>.
- Mishael, J., Morato, P.G., & Rigo, P. (2023). Numerical fatigue modeling and simulation of interacting surface cracks in offshore wind structural connections. *Marine Structures*, 92, 103472. <https://doi.org/10.1016/j.marstruc.2023.103472>.

- Mishra, R., Burela, R.G., & Pathak, H. (2019). Crack interaction study in piezoelectric materials under thermo-electro-mechanical loading environment. *International Journal of Mechanics and Materials in Design*, 15, 379-412. <https://doi.org/10.1007/s10999-018-9410-0>.
- Miteva, A. (2014). An overview of the functionally graded materials. *Machines. Technologies. Materials.*, 8(3), 13-16.
- Nusier, S.Q., & Newaz, G.M. (1998). Analysis of interfacial cracks in a TBC/superalloy system under thermomechanical loading. *Journal of Engineering for Gas Turbines and Power*, 120(4), 813-819. <https://doi.org/10.1115/1.2818473>.
- Ouinias, D., Hebbar, A., Bouiadjra, B.B., Benderdouche, N., & Serier, B. (2010). Interaction effect crack–interfacial crack using finite element method. *Materials & Design*, 31(1), 375-381. <https://doi.org/10.1016/j.matdes.2009.06.013>.
- Pant, M., Singh, I.V., & Mishra, B.K. (2010). Numerical simulation of thermo-elastic fracture problems using element free Galerkin method. *International Journal of Mechanical Sciences*, 52(12), 1745-1755. <https://doi.org/10.1016/j.ijmecsci.2010.09.008>.
- Pant, M., Singh, I.V., & Mishra, B.K. (2011a). A numerical study of crack interactions under thermo-mechanical load using EFGM. *Journal of Mechanical Science and Technology*, 25, 403-413. <https://doi.org/10.1007/s12206-010-1217-3>.
- Pant, M., Singh, I.V., & Mishra, B.K. (2011b). Evaluation of mixed mode stress intensity factors for interface cracks using EFGM. *Applied Mathematical Modelling*, 35(7), 3443-3459. <https://doi.org/10.1016/j.apm.2011.01.010>.
- Pasternak, I. (2012). Boundary integral equations and the boundary element method for fracture mechanics analysis in 2D anisotropic thermoelasticity. *Engineering Analysis with Boundary Elements*, 36(12), 1931-1941.
- Pathak, H. (2020). Crack interaction study in functionally graded materials (FGMs) using XFEM under thermal and mechanical loading environment. *Mechanics of Advanced Materials and Structures*, 27(11), 903-926. <https://doi.org/10.1080/15376494.2018.1501834>.
- Singh, I.V. (2005). A numerical study of weight functions, scaling, and penalty parameters for heat transfer applications. *Numerical Heat Transfer, Part A: Applications*, 47(10), 1025-1053. <https://doi.org/10.1080/10407780590926183>.
- Vivekanandan, A., & Ramesh, K. (2020). Study of crack interaction effects under thermal loading by digital photoelasticity and finite elements. *Experimental Mechanics*, 60, 295-316. <https://doi.org/10.1007/s11340-019-00561-9>.
- Yaghi, A., & Becker, A. A. (2005). *State of the art review: Weld simulation using finite element methods*. National Agency for Finite Element Methods and Standards, UK.
- Yan, X., & Miao, C. (2012). Interaction of multiple cracks in a rectangular plate. *Applied Mathematical Modelling*, 36(11), 5727-5740. <https://doi.org/10.1016/j.apm.2011.12.060>.
- Zhang, J.P., Wang, S.S., Gong, S.G., Zuo, Q.S., & Hu, H.Y. (2019). Thermo-mechanical coupling analysis of the orthotropic structures by using element-free Galerkin method. *Engineering Analysis with Boundary Elements*, 101, 198-213. <https://doi.org/10.1016/j.enganabound.2019.01.011>.

